AFRL-RD-PS-
TP-2022-0007

AFRL-RD-PS-
TP-2022-0007

MODELING THE FERROMAGNETIC RESONANCE RESPONSE OF A MAGNETITE NANOCRYSTAL USING BOTH MATHEMATICAL FIRST PRINCIPLES AND UBERMAG SOFTWARE

1st Lt Michael Sherburne and Dr. Vladimir Safonov

17 May 2022

Technical Paper

AIR FORCE RESEARCH LABORATORY
Directed Energy Directorate
3550 Aberdeen Ave SE
AIR FORCE MATERIEL COMMAND
KIRTLAND AIR FORCE BASE, NM 87117-5776

NOTICE AND SIGNATURE PAGE

Using Government drawings, specifications, or other data included in this document for any purpose other than Government procurement does not in any way obligate the U.S. Government. The fact that the Government formulated or supplied the drawings, specifications, or other data, does not license the holder or any other person or corporation; or convey any rights or permission to manufacture, use, or sell any patented invention that may relate to them.

Qualified requestors may obtain copies of this report from the Defense Technical Information Center (DTIC) (`http://www.dtic.mil`).

AFRL-RD-PS-TP-2022-0007 HAS BEEN REVIEWED AND IS APPROVED FOR PUBLICATION IN ACCORDANCE WITH ASSIGNED DISTRIBUTION STATEMENT.

SHERBURNE.MICHAEL.D.1050457466 Digitally signed by SHERBURNE.MICHAEL.D.1050457466 Date: 2022.09.29 10:51:50 -06'00'

1ST LT MICHAEL SHERBURNE
Predictive Effects Project Deputy
AFRL/RDHE

DORLAC.LUKE.JEROME.1385309259 Digitally signed by DORLAC.LUKE.JEROME.1385309259 Date: 2022.09.29 20:55:33 -06'00'

CAPTAIN LUKE DORLAC
Branch Chief
AFRL/RDHE

This report is published in the interest of scientific and technical information exchange, and its publication does not constitute the Government's approval or disapproval of its ideas or findings.

REPORT DOCUMENTATION PAGE

Form Approved

OMB No. 0704-0188

1. REPORT DATE *(DD-MM-YYYY)*	**2. REPORT TYPE**	**3. DATES COVERED** *(From - To)*
17-05-2022	Technical Paper	07-20-2021 to 05-17-2022

4. TITLE AND SUBTITLE

Modeling the Ferromagnetic Resonance Response of a Magnetite Nanocrystal Using Both Mathematical First Principles and Ubermag Software

5a. CONTRACT NUMBER

FA8650-16-D-5404

5b. GRANT NUMBER

5c. PROGRAM ELEMENT NUMBER

6. AUTHOR(S)

Michael Sherburne* Vladimir Safonov**

5d. PROJECT NUMBER

5e. TASK NUMBER

5f. WORK UNIT NUMBER

7. PERFORMING ORGANIZATION NAME(S) AND ADDRESS(ES)

Air Force Research Laboratory*
High Powered Electromagnetics Division
3550 Aberdeen Ave SE
Kirtland AFB, NM 87117-5776

Azimuth Corp**
2970 Presidential Dr, Unit 200
Beavercreek, OH 45324

8. PERFORMING ORGANIZATION REPORT NUMBER

AFRL-RD-PS-TP-2022-0007

9. SPONSORING/MONITORING AGENCY NAME(S) AND ADDRESS(ES)

Air Force Research Laboratory
Materials Directorate
5135 Pearson Road, Building 10
WPAFB, OH 45433

10. SPONSOR/MONITOR'S ACRONYM(S)

AFRL/RX

11. SPONSOR/MONITOR'S REPORT NUMBER(S)

12. DISTRIBUTION/AVAILABILITY STATEMENT

Distribution statement A approved for public release; distribution is unlimitedPublic Affairs release approval AFRL-2022-3572.

13. SUPPLEMENTARY NOTES

14. ABSTRACT

Magnetic nanoparticles exposed to radio-frequency (RF) fields have a wide variety of uses. A magnetic nanoparticle called magnetite nanocrystal (iron oxide - $\mathrm{Fe_3O_4}$) is showing promise in the following industries: semiconductor, medical, electronics, criminal forensics, and civil infrastructure. RF modeling is required to effectively implement these magnetite nanocrystals for both present and future applications. Prior work has performed analysis at low frequencies (kilohertz to megahertz) and established models easily accessible and free for researchers. However, easily accessible and free models for the gigahertz spectra are not available. This technical paper addresses these issues by demonstrating both a first principles model and the use of a finite difference time domain (FDTD) code called Ubermag that reproduces experimental results for the RF response of magnetite nanocrystals in the gigahertz region. RF engineers can use these models when designing magneto-optic sensors using magnetic nanocrystals, optimizing the material parameters when designing magnetic nanomaterials for de-icing applications, RF curing of polymer, and any other applications that takes advantage of the magnetic nanocrystals' magnetic response in the gigahertz spectra.

15. SUBJECT TERMS

ferromagnetic resonance; micromagnetics; modeling; nanocrystals; nanoparticles; Object Oriented Micromagnetic Framework; spintronics; Ubermag

16. SECURITY CLASSIFICATION OF:			**17. LIMITATION OF ABSTRACT**	**18. NUMBER OF PAGES**	**19a. NAME OF RESPONSIBLE PERSON**
a. REPORT	**b. ABSTRACT**	**c. THIS PAGE**			1st Lt Michael Sherburne
UNCLASSIFIED	UNCLASSIFIED	UNCLASSIFIED	SAR	40	**19b. TELEPHONE NUMBER** *(include area code)*

TABLE OF CONTENTS

Section **Page**

LIST OF FIGURES

Figure **Page**

LIST OF TABLES

Table **Page**

1.0 INTRODUCTION

Magnetic nanoparticles exposed to radio-frequency (RF) fields have a wide variety of uses. Specifically, iron oxide nanocrystals ($\mathrm{Fe_3O_4}$ - also known as magnetite) are showing promise in areas such as: RF curing of polymer in comparison to ultraviolet (UV) curing [2], medical applications [3, 4], transformer core materials [5–7], criminal forensics [8], temperature sensing [9], de-icing of roads [10], and magnetic field sensing [11]. Thus, with the numerous present applications and more to be expected in the future, the ability to model magnetite nanocrystal's RF response would be useful for RF engineers. Previous literature has characterized the material's response in the kilohertz to megahertz regime in detail [12–14]. However, there is a lack of information in regards to RF models in the gigahertz spectra. In response to this, two models are presented in this paper that are both relatively simple and free for engineers to use. The first model comes from first principles and the second model makes use of an open-sourced micromagnetics (magnetic field modeling at small length scales) code called Ubermag. Both of these models will be compared to experimental data provided by the referenced paper [1]. Any RF engineer can make use of these models to get an approximate resonance RF peak (ferromagnetic resonance, FMR) to design and predict the RF response of their magnetite nanocrystals. The FMR peak is the frequency where most of the RF heating occurs. These RF models can also be used for other magnetic nanocrystals.

Magnetic materials can experience a high frequency resonance loss, known as the FMR, when an incident alternating current (AC) magnetic field (H-field) is applied at the right frequency. In addition, an applied direct current (DC) H-field can be used to optimize the FMR's response for higher heating losses. This FMR occurs from the gyromagnetic precessional motion of electrons in the magnetic material. An applied AC response (whether a pulsed or a continuous wave) applied at the right frequency would excite an oscillation of the electrons about the directional axis of the applied H-field. These electrons oscillate from outside the axis towards the axis center. One can think that electrons further away from the axis have a higher H-field while the closer they get to the axis they have a smaller H-field. How fast these electrons oscillate back towards a relaxed state is determined by a damping coefficient (α). This physical phenomena can also be thought of as changing torque over time on the electrons.

The FMR response is represented by the Landau-Lifshitz-Gilbert (LLG) equation shown as $\frac{\partial \mathbf{M}}{\partial t} = \gamma_G[\mathbf{M} \times \mathbf{H}_{eff}] - \frac{\alpha_G}{|M|}[\mathbf{M} \times \frac{\partial \mathbf{M}}{\partial t}]$. Where $\mathbf{H}_{eff}$ is related to the magnetic flux density as $\mathbf{B} = \mu_0 \mathbf{H}_{eff}$ and μ_0 is the permeability of a vacuum ($4\pi \times 10^{-7}$ NA^{-2}. In addition, γ_G is the gyromagnetic ratio, α_G is the damping constant, and M is the magnetization field. The precessional motion of the vectors in the LLG equation are illustrated in Fig. 1. The derivation of this equation can be seen in APPENDIX A.

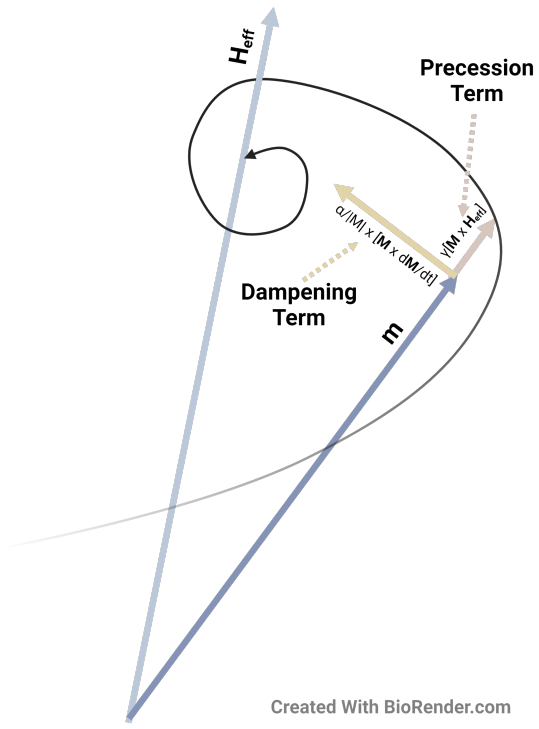

Figure 1. Illustration of the gyromagnetic precessional motion for electrons exposed to an incident magnetic field. Each aspect of the LLG equation ($\frac{\partial \mathbf{M}}{\partial t} = \gamma_G[\mathbf{M} \times \mathbf{H}_{eff}] - \frac{\alpha_G}{|M|}[\mathbf{M} \times \frac{\partial \mathbf{M}}{\partial t}]$) is labeled here.

2.0 FIRST PRINCIPLES MODELING

This section goes over the derivation of the first principles model. Modeling the FMR of magnetic nanoparticles can be done by using a modified form of the LLG equation (Eqn. 14). Since an electron has negative charge, a negative sign can be added in front of γ, which in turn would also change the sign for the $\alpha/|\mathbf{M}|$ term. In addition, the magnetization ($|\mathbf{M}|$) is equivalent to the magnetization saturation (M_s). This modified LLG formula is shown as:

$$\frac{\partial \mathbf{M}}{\partial t} = -\gamma \mathbf{M} \times \mathbf{H}_{eff} + \frac{\alpha}{M_s} \mathbf{M} \times \frac{\partial \mathbf{M}}{\partial t} \tag{1}$$

where γ is the gyromagnetic ratio, α is dimensionless damping parameter, and $\mathbf{H}_{eff}$ is the effective magnetic field. One can then follow the derivations given in APPENDIX B in order to get to Eqn. 2.

$$\chi_{xx}(\omega) = \frac{\gamma M_s[\gamma(H_0 + H_K) - j\alpha\omega]}{[\gamma(H_0 + H_K) - j\alpha\omega]^2 - \omega^2} \tag{2}$$

Eqn. 2 shows the magnetic susceptibility χ in terms of the applied AC H-field frequency (shown as the radial frequency ω). The magnetic susceptibility has both a real part and an imaginary part, where the imaginary part is proportional to the amount of energy loss. This energy loss is then proportional to the amount of heating of the nanoparticle. In addition, the DC H-field components are shown as H_0 (applied DC H-field) and H_K (magnetic anisotropy field - derived from material parameters as shown in APPENDIX B). Since usually centimeter-gram-second (CGS) units are used to collect material parameter measurements, there is a need to divide Eqn. 2 by 4π to place it in the International Systems of Units (SI) system. This is shown in Eqn. 3.

$$\chi_{xx}(\omega) = \frac{\gamma M_s[\gamma(H_0 + H_K) - j\alpha\omega]}{(\gamma(H_0 + H_k) - j\alpha\omega)^2 - \omega^2} \frac{1}{4\pi} \tag{3}$$

Eqn. 2 allows one to calculate the FMR of an magnetite nanocrystal from first principles when material parameters are given in CGS units. Of note, Eqn. 3 is meant for a specific direction along a material's crystal axis. In materials science, the crystal axis is defined as three numbers that relate to a given 3D plane X, Y, Z direction that are placed in between square brackets (e.g. [100] which points along the x-axis direction of a crystal). In order to avoid confusing readers that these square brackets are citations, this paper will show crystal axes directions with curly brackets instead (e.g. {100}). Eqn. 3 is meant for the {100} direction in a crystal axis. For the {111} direction, the reader is encouraged to read the first principle's derivation in APPENDIX D.

For any magnetite nanocrystal, the orbital momentum could change and thus, changing the g-factor in Eqn. 8. This would then change γ. In literature, a common γ for $\mathrm{Fe_3O_4}$ nanoparticles is 2.8 MHz/Oe [1]. This assumes that the g-factor in Eqn. 8 is equal to two. In addition, this value of two for the g-factor assumes that there is one Fe^{2+} ion for every two Fe^{3+} ions in the formation of $\mathrm{Fe_3O_4}$ nanoparticles. However, this is not always the case as when a magnetite nanocrystal forms and grows, it can experience imperfections in its crystal structure. These imperfections can cause the formation of different ratios of Fe^{2+} and Fe^{3+} species which can change the value of the g-factor. Other researchers have looked into the g-factor for $\mathrm{Fe_3O_4}$ nanoparticles and calculated values different than the standard value of two because of the iron oxidation changes in their experiments [15, 16].

In order to check that Eqn. 3 yields desired results, experimental data were used to replicate results in the referenced paper [1]. The following parameters from the paper were used for a $\mathrm{Fe_3O_4}$ spherical nanocrystal: $H_{int} = 177$ Oe, $\alpha = 0.254$, $r = 7.5$ nm, $K_1 = -1.36 \times 10^4$ Jm^{-3}, $\rho = 5.18$ gcm^{-3}, $M_s = 102.24$ emu/g, and $H_0 = 1$ kOe. In addition, $K = K_1/2$ is used to get a mean orientation value of the magnetic anisotropy due to the assumption of using randomly distributed magnetic anisotropy directions. H_K is solved by using the formula $H_K = 2K/M_s$. These values can now be used in Eqn. 3 to get Fig. 2.

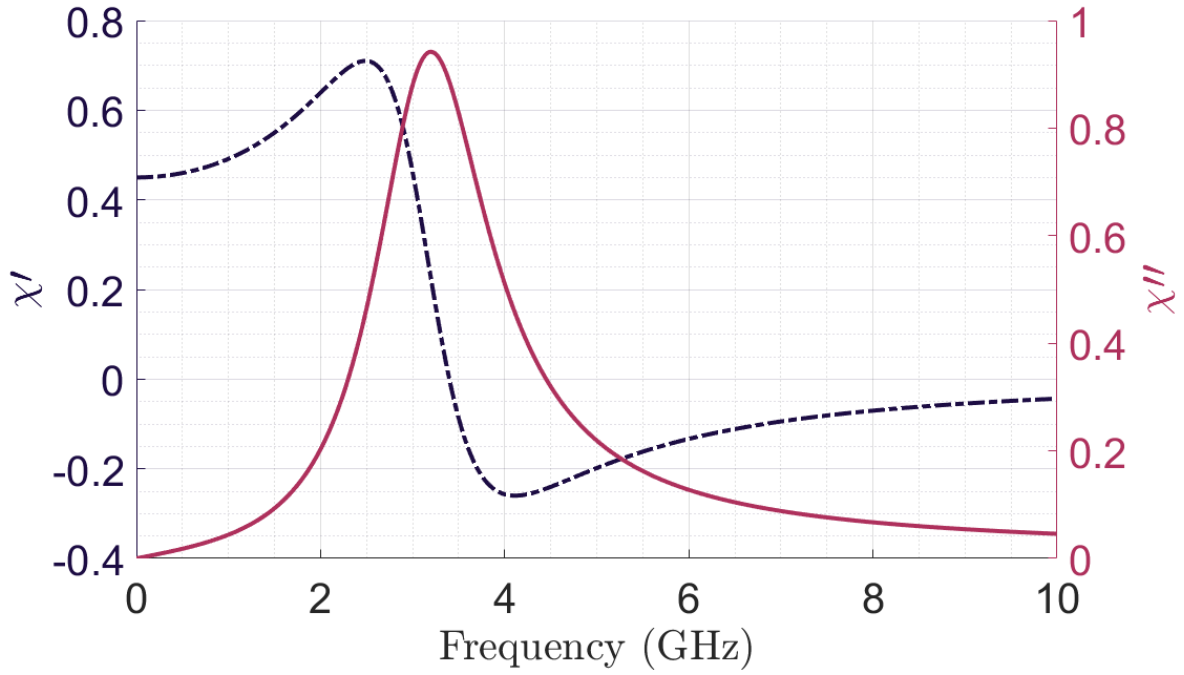

Figure 2. **Plot of both real (χ') and imaginary (χ'') magnetic susceptibilities. This comes from using the first principles model as derived in Eqn. 3 using experimental data provided from the referenced paper [1].**

By taking the fast Fourier transform (FFT) power of Eqn. 3, one can emulate data in the referenced paper [1]. The FFT power is given as,

$$P(f) = \sqrt{|\chi(f)|^2} \tag{4}$$

To place emphasis on the importance of having the same FMR and shape, the susceptibility values are normalized to its maximum value. In addition, the values are scaled by a factor of 0.6 to match the normalized maximum of the referenced paper. The referenced paper does not give any explanations into why the highest value is 0.6 and is thus, arbitrary. This replication of the paper's plot by using the first principles model can be seen in Fig. 3.

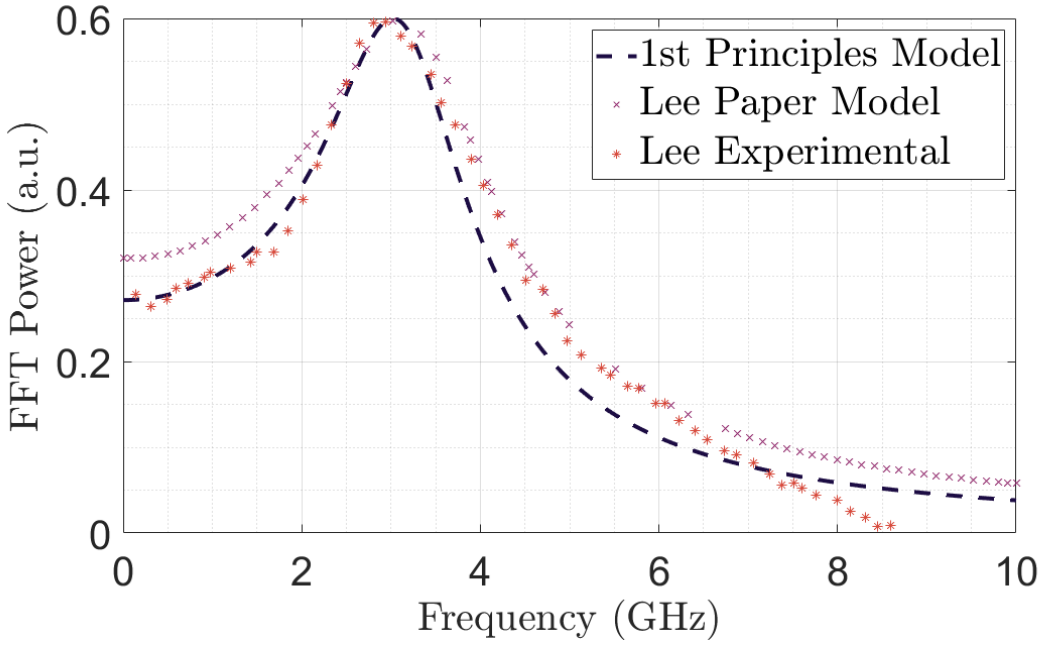

Figure 3. **Lee's data inserted into the first principles model and its magnetic susceptibility output compared against data in the referenced paper [1].**

Comparing first principles model to the referenced text in Fig. 3, a good agreement can be seen between the first principles model and the referenced paper's plot. Both plots have similar shapes and the same FMRs (3.0 GHz). The main take away is that the first principles model can accurately describe the frequency of the FMR peak of a magnetite nanocrystal as both are 3.0 GHz. In terms of error, Lee's model at 0 GHz is showing a normalized FFT power of 0.3201 which is off by 17.9% error when compared to both the first principles model and Lee's experimental results (normalized FFT power of ≈0.2716). On average, after 3.4 GHz, the first principles model is off by 19.2% from the experimental results. Therefore, the first principles model is acceptable since both Lee's model and the first principles model have similar errors depending on which side of the FMR peak the models are simulating. Regardless, both models can accurately determine the peak FMR frequency.

In addition, the first principles model needs to be checked against additional information from the referenced paper in terms of changing the H_{DC} field at a specific frequency. The figure to replicate can be seen in Fig.4. This figure shows how the temperature increase changes across varying applied $\mathrm{H_{DC}}$ fields at a specific frequency (in this case 2.5 GHz). As the magnetite nanocrystals are excited closer towards their FMR response, they heat up faster. The reader is encouraged to read the rest of the supplementary section for the other frequency cases (1.5 GHz and 2.0 GHz) and the experimental setup [1].

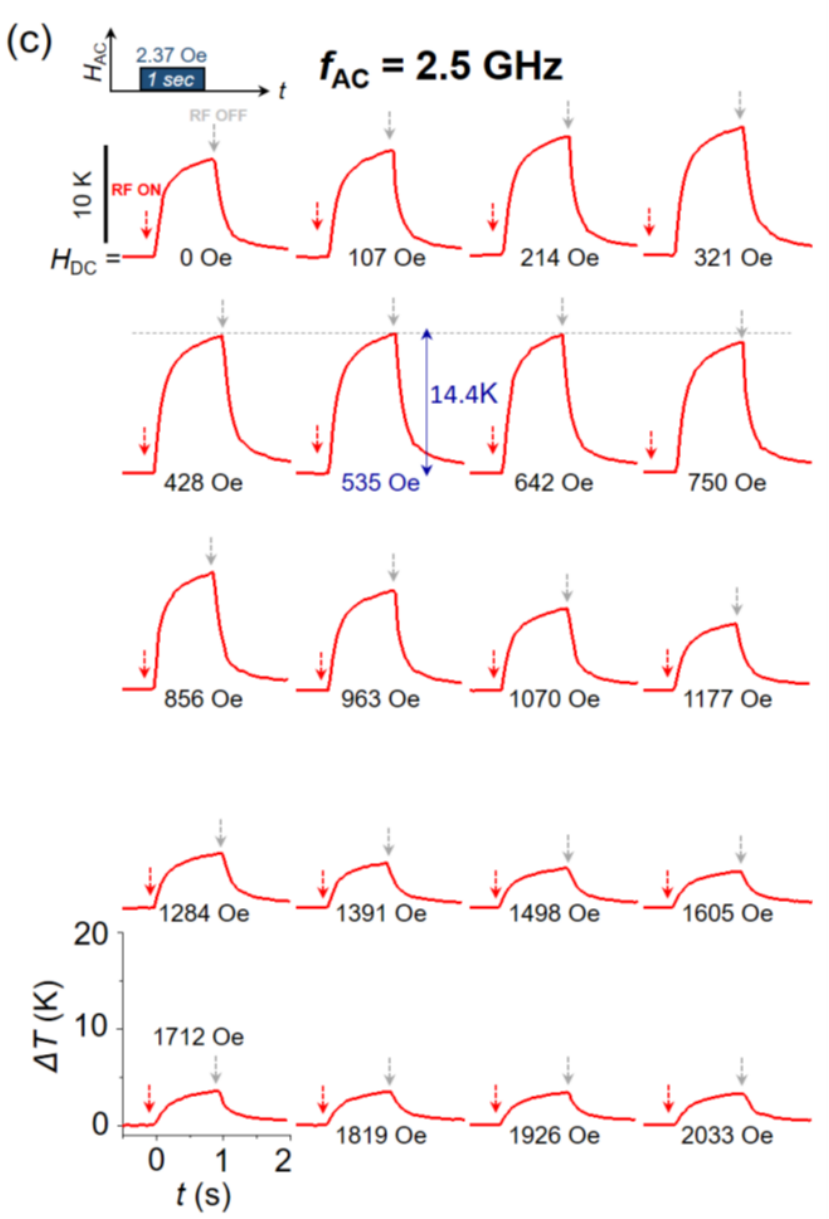

Figure 4. **Lee's experimental data showing the temperature change of magnetite nanocrystals at RF excitation of 2.5 GHz across various $\mathrm{H_{DC}}$ components.**

Replicating Fig. 4 verbatim is impossible with the first principles model due to temperature values that are dependent on the overall system (e.g. interaction effects between nanocrystals). An ideal replication could be possible by collecting experimental data of the FMR peak at various frequencies and also at various material temperatures. Fortunately, the magnitudes of the temperature increase for each $\mathrm{H_{DC}}$ field can be approximately emulated as temperature is proportional to the magnitude of the magnetic susceptibility. This emulation can be seen in Fig. 5.

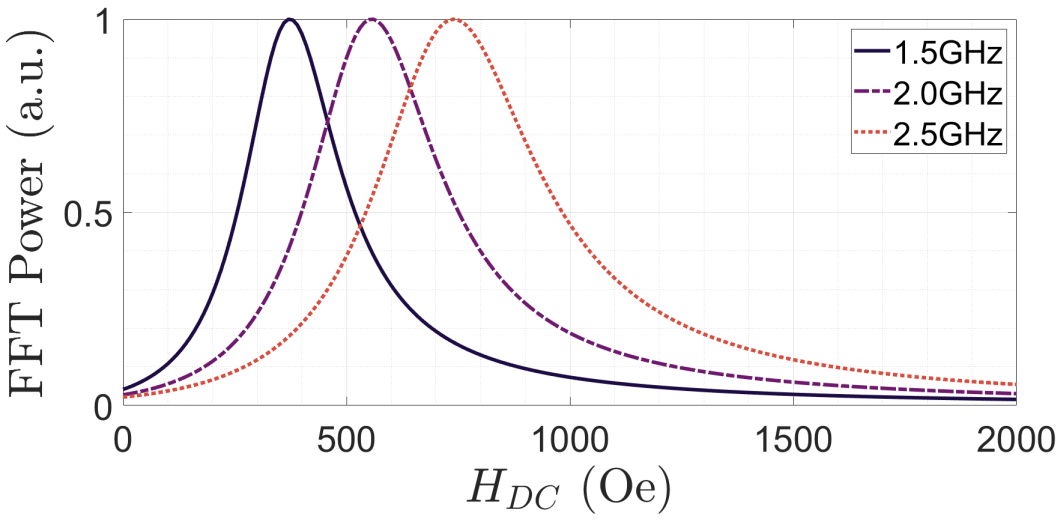

Figure 5. **First principles model calculating the FFT power of a 15 nm diameter magnetite nanocrystal with H_{AC} excitation frequencies at 1.0 GHz, 2.0 GHz, and 2.5 GHz in relation to varying H_{DC} static fields.**

The FMR peak outputs from Fig.5 were compared in Tab. 1 to the referenced paper's results. Since the reference has their experimentally measured results with coarse step sizes, a range of values about the H_{DC} value that yields the highest temperature change was used for comparison. The difference between the first principles method FFT power peak's result and the closest thermal peak H_{DC} in the reference's experimental results was considered the error.

The error for the first principles model across each of the tested frequencies: 1.0 GHz, 2.0 GHz, and 2.5 GHz is shown in Tab. 1.

Excitation Frequency (GHz)	1st Principles Peak (Oe)	Lee's Peak (Oe)	Error (Oe)
1.5	373	214-428	0
2.0	557	321-535	22
2.5	741	428-642	99

Table 1. **Comparison of the H_{DC} locations of the peak powers with respect to change in frequency for both the first principles and the experimental results from the reference.**

It can be seen that Fig. 5 reproduces $\mathrm{H_{DC}}$ which correlates to the highest temperature rise in Fig. 4 for the 1.5 GHz case. As the frequency is increased to 2.0 GHz and 2.5 GHz, the error grows as shown in Tab. 1. While magnetic susceptibility correlates to energy loss, and therefore temperature increase, it is a rough approximation due to inter-particle interactions. These interactions occur at both the overall system level and the ambient environment. The experimental results show that as the frequency increases, the temperature difference increases. The higher the temperature increases, the more it affects the resonant frequency of the overall system. For example, the

warmer the magnetite nanocrystals are, the more their inherent magnetic response will be affected. This is because the magnetic response of a magnetic material decreases as the temperature increases. Thus, there is a non-linear effect at play here. The first principles model assumes the magnetite nanocrystals are not affected by temperature changes. Therefore, with these limitations in mind, the first principles model is deemed accurate for getting an approximate $\mathrm{H_{DC}}$ value which correlates to the highest change in temperature at a given frequency. As a work around to the non-linear heating, a scaling factor derived from empirical data as shown in Fig. 4 could be used to calibrate the first principles model to the non-linear heating trend.

3.0 UBERMAG MODELING

The first principles model can be implemented in Ubermag to evaluate magnetite nanocrystals. In addition, the first principles model can be compared to Ubermag's results. Ubermag is a Python based, open source simulation software of the Object Oriented Micromagnetic Framework (OOMMF) code [17]. In order to use Ubermag correctly, all CGS units in literature have to be converted over to SI units. These conversions can be read in APPENDIX C. In addition, the gyromagnetic ratio is shown in different types of formats in literature. To go from CGS to SI units for the gyromagnetic ratio, one must determine how the gyromagnetic ratio is shown in the article. Then one can apply the conversion to SI units. The conversion to go from CGS units to SI units for Ubermag is $\gamma_0 = 2\pi\mu_0\frac{\gamma_{0_e}}{1+\alpha^2}$. γ_{0_e} is the gyromagnetic ratio given in CGS units. The proof for this conversion can be seen in APPENDIX E.

Before doing any numerical modeling, the physical step size for a magnetic volume (unit cell) needs to be less than the exchange length (l_{ex}) in order to prevent numerical error. Within an overall magnetic volume, there are magnetic interactions that occur due to magnetic moments within the volume interacting with each other. The physical lengths that these magnetic moments can interact with each other are represented by the magnetic exchange lengths (l_{ex}). These are determined by the competition between the relative strength of exchange and self-magnetostatic energies. The exchange length is given by Eqn. 5

$$l_{ex} = \sqrt{\frac{2A_{ex}}{\mu_0 M_s^2}} \tag{5}$$

where A_{ex} is the exchange energy, M_s is the saturation magnetization, and μ_0 is the permeability of a vacuum [18]. Once the exchange length is known, one can split up the overall volume into magnetic sub-volumes which are smaller than l_{ex}. This would then allow the micromagnetic model to then accurately capture the interactions between magnetic sub-volumes [19].

Experimentation has proven that numerical modeling of magnetic nanoparticles typically needs to be four unit cells. To support this claim, this section will go over a scenario that

looks at the FFT power frequency peaks of a 15 nm diameter magnetite nanocrystal. A H_{DC} field is applied at 1000 Oe. The magnetic response of the particle is simulated for 100 ns with 2,000 time steps using a sinc pulse excitation. In addition, the following number of unit cells are then modeled: two, four, 10, and 20 unit cells. Additional magnetite nanocrystal material parameters (provided by the referenced paper) are: M_s is 102.24 emu/g ($529,603.2$ A/m), α is 0.246, K is 6.8×10^3 Jm^{-3}, γ_0 is 2.64 MHz/Oe, simulation temperature is 0 K, A_{ex} is 13.2×10^{-12} J/m, and H_{AC} is 5 Oe [1]. The exchange length of this magnetite nanocrystal calculated by using Eqn. 5 is 8.65 nm. Thus, a single unit cell cannot be simulated since the diameter of the nanocrystal (15 nm) is larger than the exchange length (8.65 nm).

In addition, this scenario will also look at how long it takes to simulate each step size. The number of CPU cores used is 12 with 24 threads at a 4.15 GHz clock speed (model: AMD Ryzen 9 3900XT). Tab. 2 goes over the frequency peaks and the amount of time it took to run the simulation for each unit cell case.

Unit Cells	Frequency Peak (GHz)	Simulation Time (Minutes)
2	3.08	1.58
4	3.01	5.79
10	3.05	38.35
20	3.05	479.10

Table 2. Simulation differences of a 15 nm magnetite nanoparticle with respect to unit cell, frequency peak, and simulation time. The frequency peak starts to converge at around 10 unit cells. However, this comes at a cost in regards to simulation time which makes this impractical for more involved simulations. Thus, four unit cells is a good compromise between simulation accuracy and computational time.

Tab. 2 shows the frequency peak shifts in a "U" shaped fashion from two unit cells to 10 unit cells. The simulation converges at around 10 unit cells where no additional unit cells will improve the accuracy of the results (20 units cells from Tab. 2 produces the same value as 10 unit cells). However, the error between four unit cells and 10 unit cells is practically negligible considering that simulating practical systems of magnetite nanocrystals has interaction effects (interactions between individual nanocrystals). Therefore either simulation is useful to provide good approximations of what the magnetite nanocrystal's behavior will be. When considering computational time, 10 unit cells becomes computational expensive and not practical for more complex simulations. Consequently, the author recommends using four unit cells as it provides a good balance between accuracy and computational time.

Ubermag was then used to compare data from the referenced paper [1]. The first step is to setup the initial magnetization and geometry of the model. This can be seen in Fig. 6.

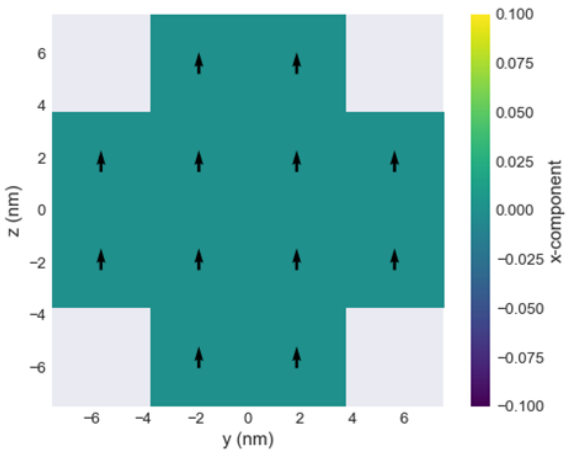

Figure 6. **Setup of the initial magnetization direction and the simulation grid in Ubermag.**

A 3D view of the simulation can be seen in Fig. 7.

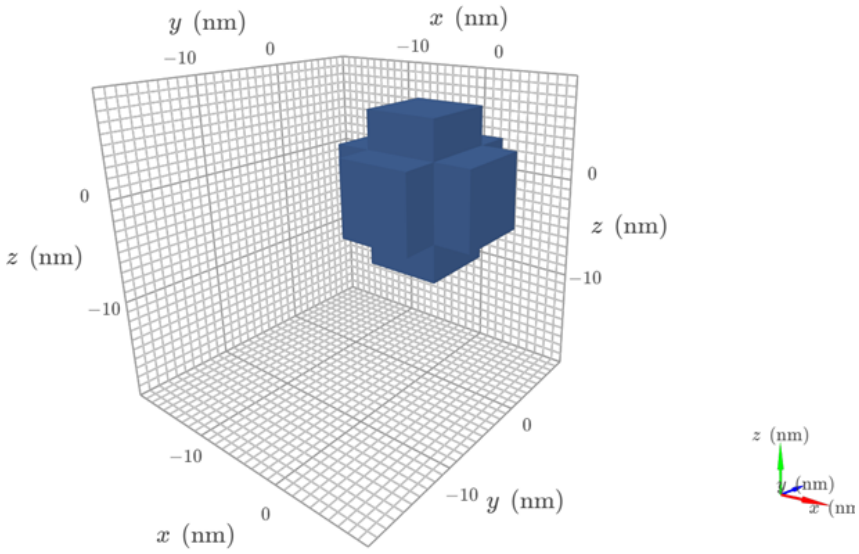

Figure 7. **3D view of the magnetite nanocrystal geometry to be simulated in Ubermag.**

The next step is to setup the model's system energy. The $\mathrm{H_{DC}}$ field is set in the Z direction. This can be seen in Fig. 8.

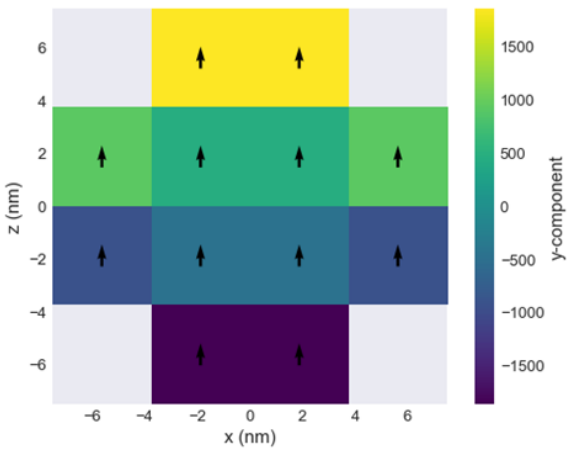

Figure 8. **Setup of the model's system energy in Ubermag.**

A sinc pulse of magnitude $\mathrm{H_{AC}}$ is then applied in the X direction. This is orthogonal to the $\mathrm{H_{DC}}$ field.

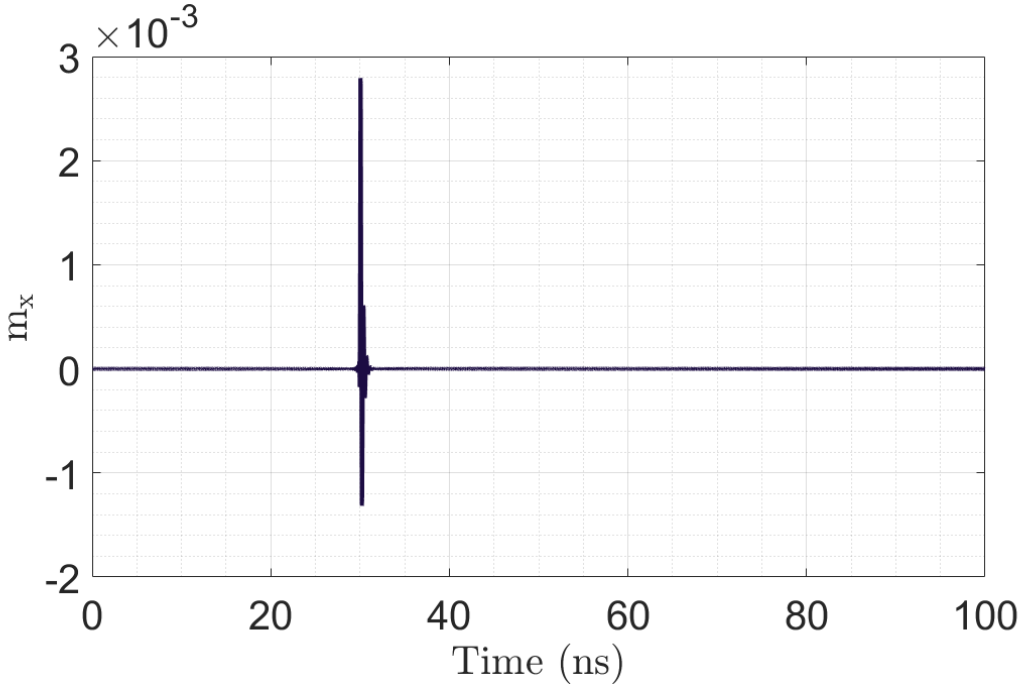

Figure 9. **Output of the m_x value in Ubermag showing a sinc pulse excitation.**

The results of the m_x component can be seen in Fig. 10.

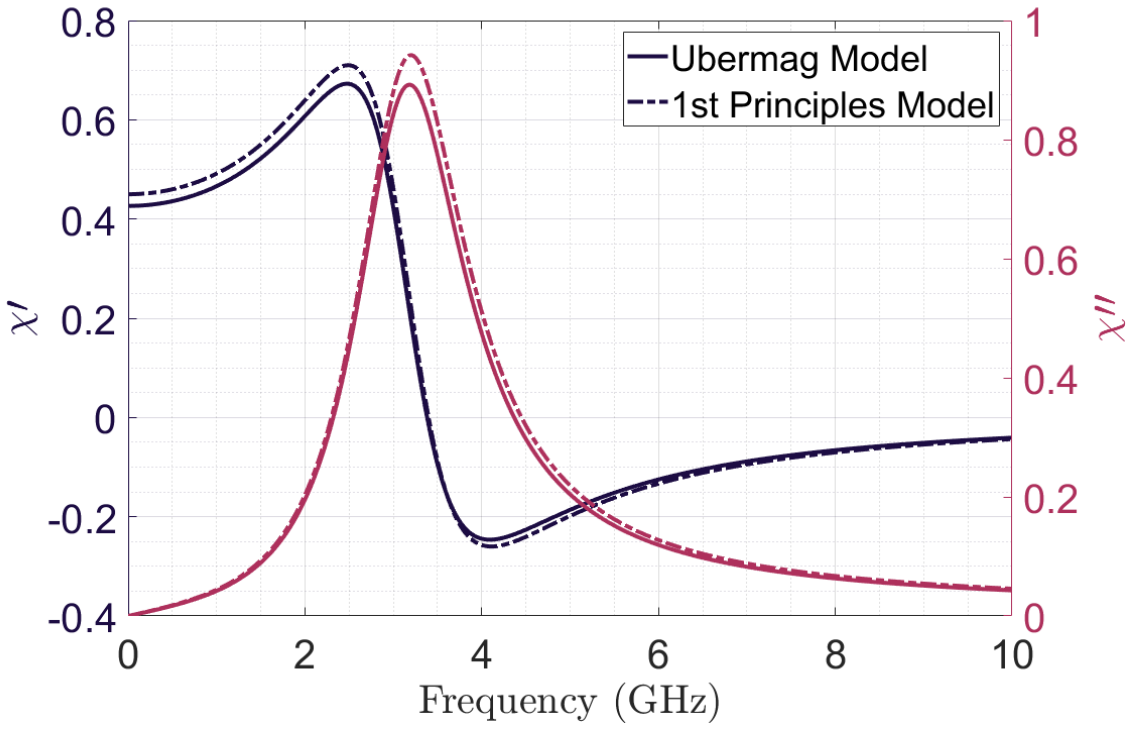

Figure 10. **Plot of the real and imaginary susceptibility (χ) of m_x Ubermag model (solid lines) overlayed over the first principles model's results (dashed lines).**

Of note, Fig. 10 produced by Ubermag is practically the same as Fig. 2 from first principles. Both of their FMR peaks are equivalent with 3.20 GHz and 3.18 GHz χ'' frequency peaks for both the first principles and Ubermag models respectively. The differences in magnitudes (5.3% for the χ' and 5.2% for the χ'') between the two models can be attributed to the first principles model assuming uniform rotation across the entire volume versus the Ubermag model breaking up the rotations into sub-particles. The near perfect agreement between the two models suggests that the models are correct and agree with Lee's empirically collected data. Finally, the FFT power response can calculated, which produces Fig. 11.

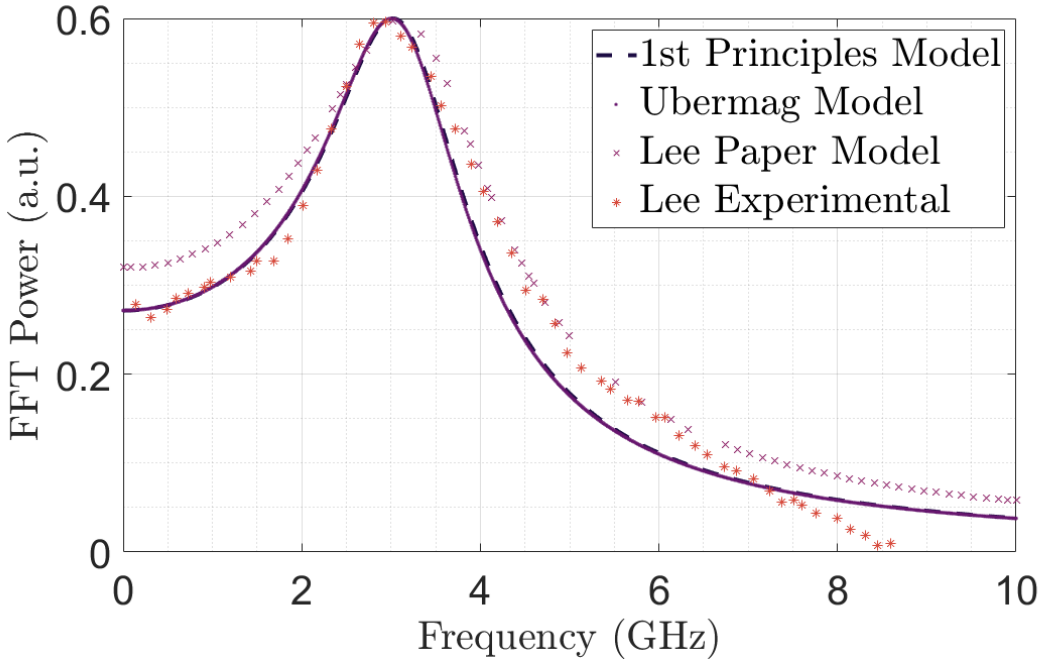

Figure 11. Plot of FFT power of the magnetic susceptibility of m_x using Ubermag and first principles models.

The experimental measurement agrees well with both the first principles and Ubermag models below the FMR peak of 3 GHz. However, beyond 3 GHz, the models diverge and none of them (including Lee's model using finite-element micromagnetics (FEMME) code) perfectly correlate with the experimental data. It is possible the measurement equipment used for the experimental data has error. In addition, it is not known why the magnitude of Lee *et al.*'s results is normalized to a maximum of 0.6 and not 1.0, which is not common practice. Hence, there may be a scaling error as well, which is the most likely explanation in regards to the higher frequency differences between the models and the experimental data. Thus, considering these circumstances, one can have confidence in both the first principles and Ubermag models for accurately predicting the FMR frequency peak of the magnetite nanoparticle when given the appropriate material parameters.

The same modeling test done for Fig. 5 for the first principles model can also be done for Ubermag. The plotted results from Ubermag (Model B) in comparison to the first principles model (Model A) can be seen in Fig. 12.

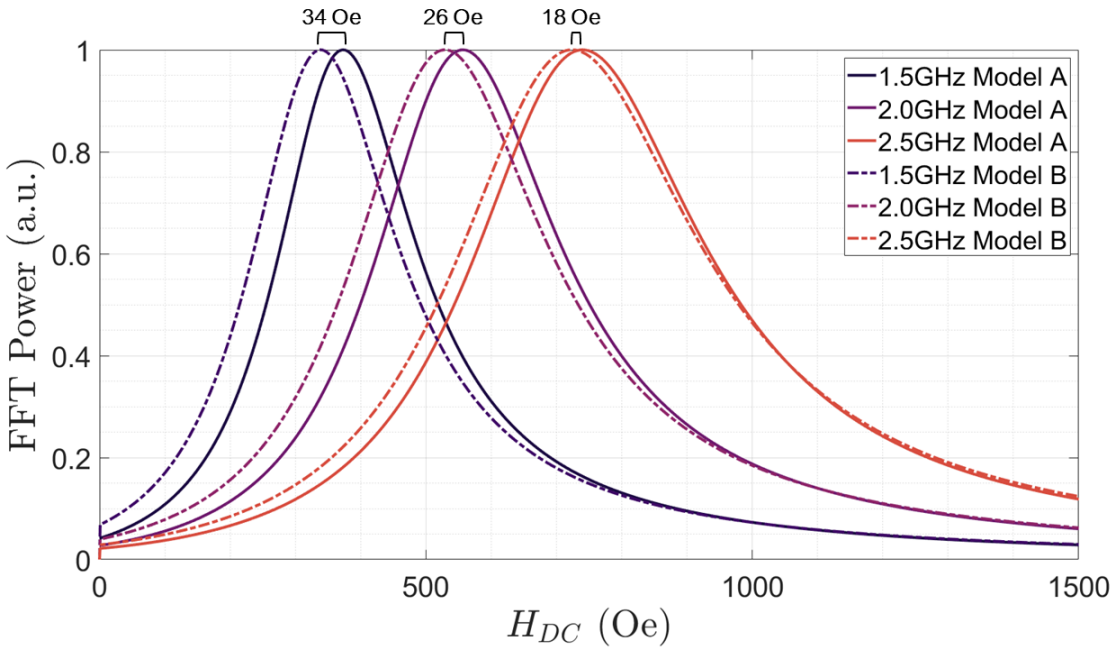

Figure 12. Change in FFT power of the magnetic susceptibility with respect to H_{DC}. Both the first principles model (Model A) and Ubermag (Model B) were plotted with varying H_{AC} excitation frequencies at 1.5 GHz, 2.0 GHz, and 2.5 GHz.

Next, one can compare the Ubermag model to the experimental results. This is shown in Tab. 3.

Excitation Frequency (GHz)	Ubermag Peak (Oe)	Lee's Peak (Oe)	Error (Oe)
1.5	339	214-428	0
2.0	531	321-535	0
2.5	723	428-642	81

Table 3. Comparison of the $\mathrm{H_{DC}}$ locations of the peak powers for each excitation frequency for both the Ubermag methods and experimental results. There is a closer agreement to the experimental results with the Ubermag model than there is with the first principles model.

When Tab. 3 is compared to Tab. 1, the Ubermag model better agrees with Lee *et al.*'s experimental results than the first principles model. The error being shown within the tables at higher frequencies could suggest thermal modeling error. This is most likely due to the M_s of the nanoparticles becoming smaller due to increased heating. Thus, this change in M_s can change the FMR peak of the magnetite nanocrystals. The Ubermag model does not consider thermal changes. Considering this limitation, the Ubermag model is still useful for approximating the peak H_{DC} needed to get the maximum FFT power response at different excitation frequencies when compared to the first principles model.

It can be seen in Fig. 12 that the first principles model deviates away from the Ubermag model. This can be attributed to the excitation frequency and the changing H_{DC}. The

first principles model considers uniform rotation along the entire volume and thus, does not consider other modes. Ubermag which is a numerical simulation code breaks up the volume into sub-particles. These sub-particles are randomly oriented and will respond individually to a magnetic field. This allows for additional modes that can interact with each other. Thus, the surface magnetization which influences the internal magnetization (H_{int}) value can change. However, as the frequency increases, the Ubermag model becomes closer to the first principles model. This can be due to the parameters specified in the referenced paper being specifically meant for 3 GHz. As one gets closer to this frequency, the models become more similar. This specific test is showing the limitation of the first principles model which has to be fed with empirical data for every case.

4.0 CONCLUSIONS

This paper has demonstrated both a first principles model and the use of a FDTD code called Ubermag to reproduce experimental results modeling the RF response of magnetite nanocrystals in the gigahertz region. The codes for both the first principles model written in MATLAB and the Python based Ubermag model are in APPENDIX F and APPENDIX G respectively. RF engineers can use these models when designing magneto-optic sensors using magnetic nanocrystals, optimizing the material parameters when designing magnetic nanomaterials for de-icing applications, RF curing of polymer, and any other applications that takes advantage of the magnetic nanocrystals' gyromagnetic response to high frequencies (gigahertz spectra).

ACKNOWLEDGMENTS

This material is declared a work of the U.S. Government and is not subject to copyright protection in the United States. The views expressed are those of the authors and do not reflect the official guidance or position of the United States Government, the Department of Defense or of the United States Air Force. Statement from DoD: The appearance of external hyperlinks does not constitute endorsement by the United States Department of Defense (DoD) of the linked websites, or the information, products, or services contained therein. The DoD does not exercise any editorial, security, or other control over the information you may find at these locations. The authors would like to thank both Dr. Marijan Beg and Mr. Martin Lang for their help in Ubermag. In addition, the authors would like to thank Dr. Daniel Guillete for his helpful advice in reading over this paper.

5.0 REFERENCES

[1] J.-H. Lee, B. Kim, Y. Kim, and S.-K. Kim, "Ultra-high rate of temperature increment from superparamagnetic nanoparticles for highly efficient hyperthermia," *Scientific Reports*, vol. 11, no. 1, Mar. 2021.

[2] K. J. Miller, K. N. Collier, H. B. Soll-Morris, R. Swaminathan, and M. E. McHenry, "Induction heating of FeCo nanoparticles for rapid RF curing of epoxy composites," *Journal of Applied Physics*, vol. 105, no. 7, p. 07E714, Apr. 2009.

[3] M. Soltani, M. H. Tehrani, F. M. Kashkooli, and M. Rezaeian, "Effects of magnetic nanoparticle diffusion on microwave ablation treatment: A numerical approach," *Journal of Magnetism and Magnetic Materials*, vol. 514, p. 167196, Nov. 2020.

[4] N. V. S. Vallabani and S. Singh, "Recent advances and future prospects of iron oxide nanoparticles in biomedicine and diagnostics," *3 Biotech*, vol. 8, no. 6, Jun. 2018.

[5] M. Rowe, "Superparamagnetic iron oxide and silica nanoparticles of high magnetic saturation and a magnetic core containing the nanoparticles," U.S. Patent US9 093 205B2, Jul. 28, 2015.

[6] M. Kin, H. Kura, and T. Ogawa, "Core loss and magnetic susceptibility of superparamagnetic Fe nanoparticle assembly," *AIP Advances*, vol. 6, no. 12, p. 125013, Dec. 2016.

[7] E. Langlois, J. Watt, D. Huber, M. McDonough, T. Monson, and J. Neely, "Design and evaluation of nano-composite core inductors for efficiency improvement in high-frequency power converters," in *2020 IEEE Applied Power Electronics Conference and Exposition (APEC)*. IEEE, Mar. 2020.

[8] Z. Wang, X. Jiang, W. Liu, G. Lu, and X. Huang, "A rapid and operator-safe powder approach for latent fingerprint detection using hydrophilic $\mathrm{Fe_3O_4@SiO_2-CdTe}$ nanoparticles," *Science China Chemistry*, vol. 62, no. 7, pp. 889–896, Apr. 2019.

[9] Y. Miao, B. Liu, K. Zhang, Y. Liu, and H. Zhang, "Temperature tunability of photonic crystal fiber filled with $\mathrm{Fe_3O_4}$ nanoparticle fluid," *Applied Physics Letters*, vol. 98, no. 2, p. 021103, Jan. 2011.

[10] X. Liu, Y. Zhao, W. Liu, and D. Yan, "Microwave heating and deicing efficiency for asphalt concrete with $\mathrm{SiC-Fe_3O_4}$ microwave enhanced functional layer," *Journal of Cleaner Production*, vol. 332, p. 130111, Jan. 2022.

[11] Y. Chen, Q. Han, T. Liu, W. Yan, and Y. Yao, "Magnetic field sensor based on ferrofluid and photonic crystal fiber with offset fusion splicing," *IEEE Photonics Technology Letters*, vol. 28, no. 19, pp. 2043–2046, Oct. 2016.

[12] M. Suzuki, "Ac magnetic susceptibility," University of New York, Tech. Rep., Sep. 2009.

[13] R. Rosensweig, “Heating magnetic fluid with alternating magnetic field,” *Journal of Magnetism and Magnetic Materials*, vol. 252, pp. 370–374, Nov. 2002.

[14] D. Laughlin, “Surfactant-enhanced site remediation,” ETEC LLC, Tech. Rep., 2015. [Online]. Available: https://www.mdeq.ms.gov/wp-content/uploads/2015/10/surfactant.pdf

[15] G. S. Shahane, K. V. Zipare, and R. P. Pant, “Synthesis and characterization of superparamagnetic $\mathrm{Fe_3O_4}$ nanoparticles for ferrofluid application,” *Magnetohydrodynamics*, vol. 49, no. 3-4, pp. 317–321, 2013.

[16] D. J. Huang, C. F. Chang, H.-T. Jeng, G. Y. Guo, H.-J. Lin, W. B. Wu, H. C. Ku, A. Fujimori, Y. Takahashi, and C. T. Chen, “Spin and orbital magnetic moments of $\mathrm{Fe_3O_4}$,” *Physical Review Letters*, vol. 93, no. 7, Aug. 2004.

[17] M. Beg, M. Lang, and H. Fangohr, “Ubermag: Toward more effective micromagnetic workflows,” *IEEE Transactions on Magnetics*, vol. 58, no. 2, pp. 1–5, Feb. 2022.

[18] C. Mușuroi and M. Volmer, “Oommf modelling of magnetization dynamics in micrometer sized structures for sensing applications,” in *Bulletin of the Transilvania University of BraÅov Series I: Engineering Sciences*, vol. 11, no. 1, 2018, pp. 47–54.

[19] G. S. Abo, Y.-K. Hong, J. Park, J. Lee, W. Lee, and B.-C. Choi, “Definition of magnetic exchange length,” *IEEE Transactions on Magnetics*, vol. 49, no. 8, pp. 4937–4939, Aug. 2013.

[20] J. P. Zimmerman, “Micromagnetic simulations of magnetic exchange spring systems,” Ph.D. dissertation, University of Southampton, Nov. 2007.

[21] S. Stoll, “7. angular momentum,” Online, 2021. [Online]. Available: https://easyspin.org/455/angularmomentum.html

6.0 LIST OF SYMBOLS, ABBREVIATIONS, AND ACRONYMS

AC	Alternating Current
CGS	Centimeter-Gram-Second
DC	Direct Current
FDTD	Finite Difference Time Domain
FEA	Finite Element Analysis
FEMME	Finite-Element Micromagnetics
FFT	Fast Fourier Transform
FMR	Ferromagnetic Resonance
H-Field	Magnetic Field
LLG	Landau-Lifshitz-Gilbert

OOMMF	Object Oriented Micromagnetic Framework
RF	Radio-Frequency
SI	International Systems of Units
UV	Ultraviolet

APPENDIX A LANDAU-LIFSHITZ-GILBERT EQUATION DERIVATION

To start, the equation for the angular momentum $\mathbf{L}$ of the magnetic moment $\vec{\mu}$ of a dipole in the magnetic flux density $\mathbf{B}$ is:

$$\frac{d\mathbf{L}}{dt} = \vec{\mu} \times \mathbf{B} \tag{6}$$

In quantum mechanics, the relationship between the magnetic moment and the angular momentum is determined by the relation (see, e.g., [20]):

$$\vec{\mu} = \gamma_L \mathbf{L}, \tag{7}$$

where γ_L (gyromagnetic ratio) is given as

$$\gamma_L = -g\frac{\mu_B}{\hbar} \tag{8}$$

In Eqn. 8, g is the Landé factor (also known as the g-factor), $\hbar$ is Plank's constant, and μ_B is the Bohr magnetron. The Bohr magnetron expresses the magnetic moment of an electron caused by spin angular momentum. This is shown as,

$$\mu_B = \frac{|e|\hbar}{2m_e}. \tag{9}$$

which is equal to 9.274078×10^{-24} Am^2, m_e is the mass of an electron (9.109×10^{-31} kg), e is the charge of an electron (-1.602×10^{-19} C), and $\hbar$ is Plank's constant (1.05457×10^{-34} Js). Next, both sides of Eqn. 10 are multiplied by γ_L. Then, taking into account Eqn. 7, one gets:

$$\frac{d\vec{\mu}}{dt} = \gamma_L[\vec{\mu} \times \mathbf{B}] \tag{10}$$

The total magnetic dipole moment ($\vec{\mu}$) can be expressed in terms of the magnetization ($\mathbf{M}$) and is shown as:

$$\mathbf{M} = \frac{\vec{\mu}}{V} \tag{11}$$

where V is the volume of the material. Eqn. 10 for the magnetic moment can be conveniently rewritten as the equation that describes the precession of magnetization in an effective magnetic field ($\mathbf{H}_{eff}$):

$$\frac{d\mathbf{M}}{dt} = \gamma_L \mu_0[\mathbf{M} \times \mathbf{H}_{eff}], \tag{12}$$

where $\mathbf{H}_{eff}$ is related to the magnetic flux density as $\mathbf{B} = \mu_0 \mathbf{H}_{eff}$ and μ_0 is the permeability of a vacuum ($4\pi \times 10^{-7}$ NA^{-2}. $\mathbf{H}_{eff}$. By vectorially multiply both sides of the Eqn. 12 by the magnetization vector, one gets:

$$[\mathbf{M} \times \frac{d\mathbf{M}}{dt}] = \gamma_L \mu_0 [\mathbf{M} \times [\mathbf{M} \times \mathbf{H}_{eff}]] \tag{13}$$

It can be observed that the obtained vectors in the left and right parts of Eqn. 14 are orthogonal to the precession vector and the vector of the magnetization. Thus, this resulting vector can be considered as the term responsible for the damping of the magnetization precession. In this case, the magnitude of the magnetization does not change. Next, putting precession and damping together, one gets the LLG equation in the form:

$$\frac{d\mathbf{M}}{dt} = \gamma_G [\mathbf{M} \times \mathbf{H}_{eff}] - \frac{\alpha_G}{|M|} [\mathbf{M} \times \frac{d\mathbf{M}}{dt}], \tag{14}$$

where γ_G is a gyromagnetic ratio and α_G is a damping constant. It is important to note that there are two forms of the LLG equation, which are both equivalent. Eqn. 14 is in the form of Gilberts. The other form is known as Landau-Lifshitz. The reader is encouraged to reference the cited dissertation to see the relation between the two forms [20].

In order to cause a precession of motion about an applied DC magnetic field, one must apply an external AC magnetic field that is not parallel (orthogonal gives the optimal response) to the applied DC magnetic field in accordance to the LLG formula. An external DC H-field is not required to make a magnetic nanoparticle exhibit precession and damping as these nanoparticles also contain an internal H-field which are measured from empirical data. The amount of energy the magnetic dipole moments have is linear to the applied AC magnetic field (the magnetic dipole moments align parallel to the magnetic field). This is also known as the Zeeman effect and the amount of energy of the magnetic dipole moment is shown as:

$$E = -\vec{\mu} \cdot \mathbf{B} = -|\vec{\mu}| \cdot |\mathbf{B}| \cdot \cos(\theta) \tag{15}$$

where $\vec{\mu}$ is the magnetic dipole moment, $\mathbf{B}$ is the applied magnetic field, and θ is the angle between the directions of both the magnetic dipole moment and the applied field [21]. The main takeaway from Eqn. 15 is that a stronger external AC magnetic field gives a stronger precessional magnitude response due to a magnetic dipole moment having more energy. This Zeeman term also shows up in micromagnetics code.

APPENDIX B FIRST PRINCIPLES DERIVATION

$\mathbf{H}_{eff}$ is given by

$$\mathbf{H}_{eff} = -\frac{1}{V}\frac{\partial \mathcal{E}}{\partial \mathbf{M}} \tag{16}$$

where $\mathbf{M}$ is the magnetization ($|\mathbf{M}| = M_s$) and V is the magnetic volume (ferromagnetic grain). The energy density for a particle with cubic anisotropy can be written in the form of the first order,

$$\frac{\mathcal{E}}{V} = K_c(m_z^2 m_x^2 + m_z^2 m_y^2 + m_x^2 m_y^2) - M_s(m_z H_0 + m_x h_x + m_y h_y) \tag{17}$$

Here and later $\mathbf{m} = \mathbf{M}/M_s$ is a unit vector and $m_z^2 + m_x^2 + m_y^2 = 1$. The static H_0 is directed along the z axis. Both h_x and h_y are small transverse alternating fields. The LLG Eqn. 1 can be rewritten as

$$\frac{\partial \mathbf{m}}{\partial t} = -\gamma \mathbf{m} \times \mathbf{H}_{eff} + \alpha \mathbf{m} \times \frac{\partial \mathbf{m}}{\partial t} \tag{18}$$

Next, the effective fields can be calculated along each orthogonal direction. This then obtains Eqn. 19

$$H_{eff_{x,y,z}} = -\frac{1}{M_s V}\frac{\partial \mathcal{E}}{\partial m_{x,y,z}} \tag{19}$$

,

Next, both Eqn. 19 and Eqn. 17 can be rearranged to get

$$H_{eff}, z = -\frac{K_c}{M_s}(2m_z m_x^2 + 2m_z m_y^2) + H_0 \simeq H_0, \tag{20}$$

$$H_{eff}, x = -\frac{K_c}{M_s}(2m_x m_z^2 + 2m_x m_y^2) + h_x \simeq -H_K m_x + h_x, \tag{21}$$

$$H_{eff}, y = -\frac{K_c}{M_s}(2m_y m_z^2 + 2m_y m_x^2) + h_y \simeq -H_K m_y + h_y, \tag{22}$$

where $H_K = 2K_c/M_s$. A simplification is then made in the equations given above by making $m_z \simeq 1$ and leaving only the linear terms in m_x and m_y. Thus, neglecting the quadratic terms in these components. This is because the magnetic susceptibility that is being calculated throughout this process is dimensionless, and thus m_z can be calculated as a normalized magnetic field. The cross product of two vectors is defined as

$$\mathbf{A} \times = \begin{pmatrix} \hat{\mathbf{x}} & \hat{\mathbf{y}} & \hat{\mathbf{z}} \\ A_x & A_y & A_z \\ B_x & B_y & B_z \end{pmatrix} = \hat{\mathbf{x}} \begin{pmatrix} A_y & A_z \\ B_y & B_z \end{pmatrix} - \hat{\mathbf{y}} \begin{pmatrix} A_x & A_z \\ B_x & B_z \end{pmatrix} + \hat{\mathbf{z}} \begin{pmatrix} A_x & A_y \\ B_x & B_y \end{pmatrix} = \hat{\mathbf{x}}(A_y B_z - B_y A_z) - \hat{\mathbf{y}}(A_x B_z - B_x A_z) + \hat{\mathbf{z}}(A_x B_y - B_x A_y) \tag{23}$$

where $\hat{\mathbf{x}}$, $\hat{\mathbf{y}}$, and $\hat{\mathbf{z}}$ are unit vectors. The vector product between $\mathbf{m}$ and $\mathbf{H}_{eff}$ can now be written as

$$\mathbf{m} \times \mathbf{H}_{eff} = \hat{\mathbf{x}}[m_y H_0 - (-H_K m_y + h_y) m_z] - \hat{\mathbf{y}}[m_x H_0 - (-H_K m_x + h_x) m_z] + \hat{\mathbf{z}}(m_x H_{eff,y} - H_{eff,x} m_y) \tag{24}$$

which then becomes

$$\mathbf{m} \times \mathbf{H}_{eff} = \begin{pmatrix} (H_0 + H_K) m_y - h_y \\ -(H_0 + H_K) m_x - h_x \\ 0 \end{pmatrix} \tag{25}$$

The z component is neglected since it contains only negligible quadratic terms (m_x and m_y). These orthogonal components are negligible since the magnetic field is not going through them and thus $\simeq 1$. The cross product between $\mathbf{m}$ and $\partial \mathbf{m}/\partial t$ becomes

$$\mathbf{m} \times \frac{\partial \mathbf{m}}{\partial t} = \begin{pmatrix} -\partial m_y/\partial t \\ \partial m_x/\partial t \\ 0 \end{pmatrix} \tag{26}$$

Next, both Eqn. 25 and Eqn. 26 can be plugged into Eqn. 18 in order to obtain

$$\frac{\partial m_x}{\partial t} = -\gamma(H_0 + H_K) m_y + \gamma h_y - \alpha \frac{\partial m_y}{\partial t} \tag{27}$$

$$\frac{\partial m_y}{\partial t} = \gamma(H_0 + H_K) m_x - \gamma h_x + \alpha \frac{\partial m_x}{\partial t} \tag{28}$$

Both Eqn. 27 and Eqn. 28 can be rearranged to get the following

$$\frac{\partial m_x}{\partial t} + \alpha \frac{\partial m_y}{\partial t} = -\gamma(H_0 + H_K) m_y + \gamma h_y \tag{29}$$

$$\frac{\partial m_y}{\partial t} - \alpha \frac{\partial m_x}{\partial t} = \gamma(H_0 + H_K) m_x - \gamma h_x \tag{30}$$

Next, one must consider the solutions of both Eqn. 29 and Eqn. 30 in the frequency space. The rotating components can be represented as $m_{x,y}(t) = m_{x,y}e^{-j\omega t}$ and $h_{x,y}(t) = h_{x,y}e^{-j\omega t}$. Thus, Eqn. 29 and Eqn. 30 become Eqn. 31 and Eqn. 32 respectively

$$\frac{\partial m_x e^{-j\omega t}}{\partial t} + \alpha \frac{\partial m_y e^{-j\omega t}}{\partial t} = -\gamma(H_0 + H_K)m_y e^{-j\omega t} + \gamma h_y e^{-j\omega t}, \tag{31}$$

$$\frac{\partial m_y e^{-j\omega t}}{\partial t} - \alpha \frac{\partial m_x e^{-j\omega t}}{\partial t} = \gamma(H_0 + H_K)m_x e^{-j\omega t} - \gamma h_x e^{-j\omega t}. \tag{32}$$

After applying the derivatives and cancelling exponentials in both sides, one gets to both Eqn. 33 and Eqn. 34, respectively

$$-j\omega m_x - j\alpha\omega m_y + \gamma(H_0 + H_K)m_y = \gamma h_y \tag{33}$$

$$-j\omega m_y + j\alpha\omega m_x - \gamma(H_0 + H_K)m_x = -\gamma h_x \tag{34}$$

One can then take both Eqn. 33 and Eqn. 34 and express them in matrix form to get Eqn. 35.

$$\gamma \begin{pmatrix} h_x \\ h_y \end{pmatrix} = \begin{pmatrix} \gamma(H_0 + H_K) - j\alpha\omega & j\omega \\ -j\omega & \gamma(H_0 + H_K) - j\alpha\omega \end{pmatrix} \begin{pmatrix} m_x \\ m_y \end{pmatrix} \tag{35}$$

Eqn. 35 can be rearranged to make

$$\begin{pmatrix} h_x \\ h_y \end{pmatrix} = \frac{1}{\gamma M_s} \begin{pmatrix} \gamma(H_0 + H_K) - j\alpha\omega & j\omega \\ -j\omega & \gamma(H_0 + H_K) - j\alpha\omega \end{pmatrix} \begin{pmatrix} M_s m_x \\ M_s m_y \end{pmatrix} \tag{36}$$

Using the definition of susceptibility for the rotating components $M_s m_k = \chi_{jk}(\omega)h_j$, one can write the inverse susceptibility

$$\chi_{jk}^{-1}(\omega) = \frac{h_j}{M_s m_k}. \tag{37}$$

Recalling Eqn. 36, one can compare this relation with Eqn. 37 and get the inverse susceptibility Eqn. 38.

$$\chi_{jk}^{-1}(\omega) = \frac{1}{\gamma M_s} \begin{pmatrix} \gamma(H_0 + H_K) - j\alpha\omega & j\omega \\ -j\omega & \gamma(H_0 + H_K) - j\alpha\omega \end{pmatrix} \tag{38}$$

Calculating the inverse matrix yields,

$$\chi_{jk}(\omega) = \frac{\gamma M_s}{\gamma^2(H_0+H_K)^2 + (1+\alpha^2)\omega^2 - j2\alpha\omega\gamma(H_0+H_K)} \times \begin{pmatrix} \gamma(H_0+H_K) - j\alpha\omega & -j\omega \\ j\omega & \gamma(H_0+H_K) - j\alpha\omega \end{pmatrix} \tag{39}$$

When going along the x direction, Eqn. 39 simplifies down to Eqn. 40.

$$\chi_{xx}(\omega) = \frac{\gamma M_s[\gamma(H_0+H_K) - j\alpha\omega]}{[\gamma(H_0+H_K) - j\alpha\omega]^2 - \omega^2} \tag{40}$$

In addition, since usually centimeter-gram-second (CGS) units are used to collect material parameter measurements, there is a need to divide Eqn. 40 by 4π to place it in the International Systems of Units (SI) system. This is shown in Eqn. 41.

$$\chi_{xx}(\omega) = \frac{\gamma M_s[\gamma(H_0+H_K) - j\alpha\omega]}{(\gamma(H_0+H_K) - j\alpha\omega)^2 - \omega^2}\frac{1}{4\pi} \tag{41}$$

APPENDIX C CGS TO SI UNIT CONVERSIONS

This appendix chapter is to summarize the conversions used to convert CGS units to SI units in order to use numerically model magnetic nanoparticles. Tab. C-1 summarizes these conversions.

Parameter	CGS	SI	Conversion Multiplicative Factor
γ	$\frac{Hz}{Oe}$	$\frac{m}{As}$	$\frac{4\pi}{1000}$
H	Oe	$\frac{A}{m}$	$\frac{1000}{4\pi}$
M	Oe	$\frac{A}{m}$	$\frac{1000}{4\pi}$
M_{sat}	$\frac{emu}{g}$	$\frac{A}{m}$	$\rho \times 1000$
χ	dimensionless	dimensionless	$4\ \pi$

Table C-1. Useful conversions for information in papers that are shown in CGS units and need to be converted over to SI in order to be used in numerical modeling.

APPENDIX D {111} AXIS FIRST PRINCIPLES DERIVATION

In order to calculate the susceptibility in the case of an equilibrium {111} direction, it is necessary to move from the coordinates x, y, z associated with cubic symmetry to new coordinates x', y', z', as shown in the Fig. D-1. Then, the term with cubic anisotropy is transformed to the form:

$$\begin{aligned} & K_{\mathrm{c}}\left(m_z^2 m_x^2+m_z^2 m_y^2+m_x^2 m_y^2\right) \\ = & \frac{1}{24} H_K M_s[3\left(m_{x'}^4+m_{y'}^4\right)+4 m_{z'}^4-4(m_{x'}^3+m_{y'}^3) m_{z'} \\ & +6 m_{x'}^2 m_{y'}^2+12(m_{x'}+m_{y'}) m_{x'} m_{y'} m_{z'}] \end{aligned} \tag{42}$$

Repeating the same sequence of deriving the formula for susceptibility, one arrives at the following expression:

$$\begin{aligned} \chi_{jk}(\omega) = & \frac{\gamma M_s}{\gamma^2\left(H_0-\frac{2}{3} H_K\right)^2-(1+\alpha^2)\omega^2-i 2 \alpha \omega \gamma\left(H_0-\frac{2}{3} H_K\right)} \\ & \times\left(\begin{array}{cc} \gamma\left(H_0-\frac{2}{3} H_K\right)-i \alpha \omega & -i \omega \\ i \omega & \gamma\left(H_0-\frac{2}{3} H_K\right)-i \alpha \omega \end{array}\right) \end{aligned} \tag{43}$$

It can be observed that the difference between this formula and Eqn. 39 for the coordinate system associated with the axes of the cube is only in the replacement of the anisotropy field H_K by $-2H_K/3$.

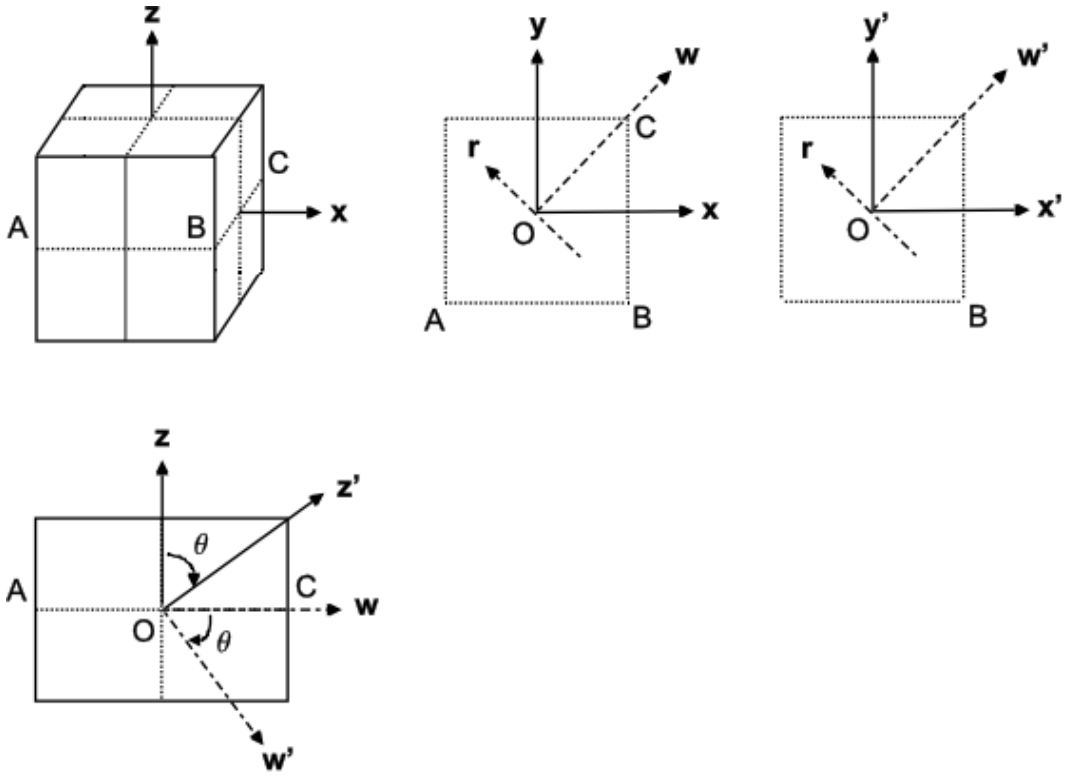

Figure D-1. Cube with 4th order axes (100), (010), (001). Rotation around the vector r at an angle θ to the third axis (111).

Using Eqn. 44, one can apply the same first principles modeling as seen in Fig. 2. The plotted results for the magnetic susceptibility is shown in Fig. D-2.

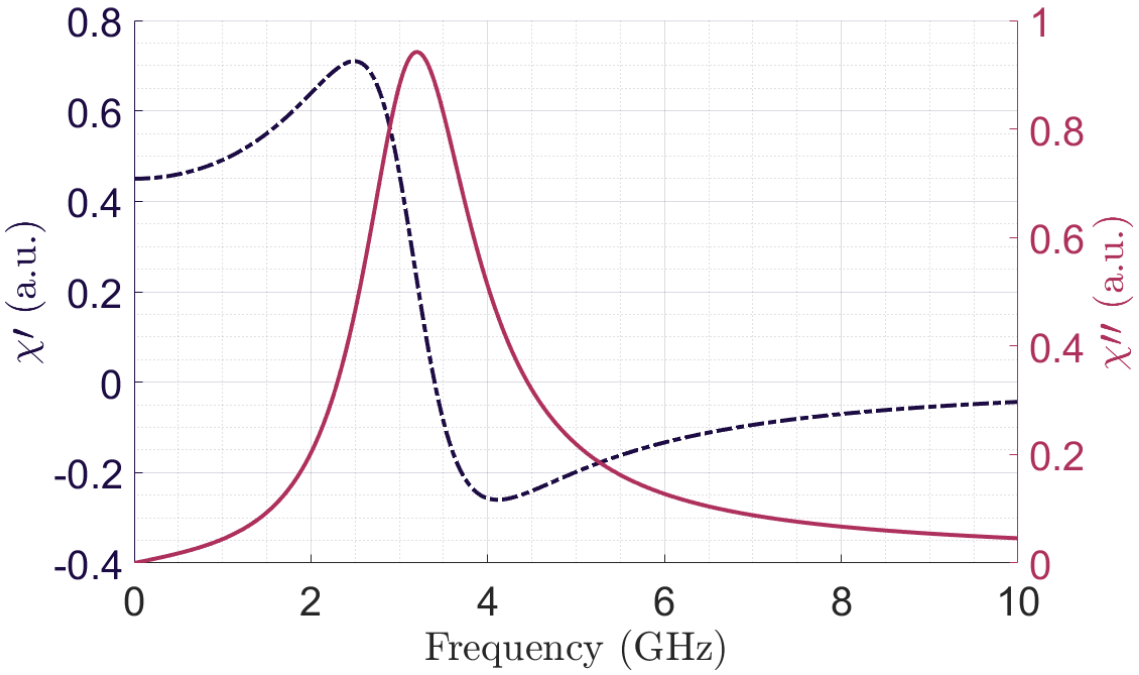

Figure D-2. Plot of both real ($\chi\prime$) and imaginary ($\chi\prime\prime$) magnetic susceptibilities. This comes from using the first principles model as derived in Eqn. 44 and using values of a magnetite spherical nanocrystal from the referenced paper [1].

Of interest, Fig. D-2 is the same as Fig. 2. This makes sense as the magnetite nanocrystal is spherical and rotating the axis will not change the inherent frequency response of the material.

APPENDIX E PROOF FOR CONVERTING GYROMAGNETIC RATIO FROM CGS TO SI UNITS

Literature such as those seen in Lee et al.'s paper sometimes report the electron gyromagnetic ratio (γ_e) in CGS units [1]. γ_e by itself is in angular frequency and its units shown as rad/sT. This is a complicated form of γ_e. Instead, a more simplified version is shown as γ_e with the units Hz/T. Sometimes this is shown as Hz/Oe in literature which relates to Hz/T by using a 10^{-4} conversion factor to get $Hz/10^{-4}T$. This version now has (γ_e) shown as ($\gamma_e/2\pi$). Researchers will also write $\gamma_e/2\pi$ as γ_0. This is not the same γ_0 used by Ubermag which uses units of m/As. In order to make this difference clearer, γ_0 will be uniquely defined from the $\gamma_e/2\pi$ representation as γ_{0_e}.

The Larmor precession frequency which models the precession of the magnetic moment of an object about an external magnetic field is shown in Eqn. 44.

$$\omega_0 = |\gamma|\mu_0 H_0 \tag{44}$$

One can divide ω_0 by H_0. The unit math is shown here:

$$\frac{\omega_0}{H_0} = \frac{2\pi\frac{rad}{s}}{\frac{A}{m}} = 2\pi\frac{m\ rad}{A\ s} = \gamma_0.$$

It is known that

$$1\frac{rad}{s} = \frac{1}{2\pi}Hz.$$

Thus,

$$\gamma_0 = \frac{mHz}{A} = \frac{m}{As}$$

$\frac{m}{As}$ is not the same $\frac{Hz}{T}$, thus the representation of γ_0 certainly changes across literature. Since $\frac{m}{As}$ is from the $\frac{\omega_0}{H_0}$ term, this now makes Eqn. 44 in the form shown in Eqn. 45.

$$\gamma_0 = \mu_0\gamma \tag{45}$$

The question now is what are the units for γ? The unit derivation is shown here: $\frac{\gamma_0}{\mu_0} = \frac{\frac{m}{As}}{\frac{kgm}{s^2A^2}} = \frac{s^2A^2m}{kgmAs} = \frac{sA}{kg} = \gamma$. This means γ in Eqn. 45 is in units of $\frac{sA}{kg}$. Now, how does one relate this version of γ to γ_0? One can first start by converting the CGS units for γ_{0_e} to SI units. The work is shown here: $\frac{Hz}{T} = \frac{\frac{1}{s}}{\frac{kg}{As^2}} = \frac{1}{s}\frac{As^2}{kg} = \frac{sA}{kg}$. Thus, γ_{0_e} is equivalent to γ in Eqn. 45. However, the conversion is not yet finished. It is known that γ_{0_e} is equal to $\frac{\gamma_e}{2\pi}$, thus $\gamma_{0_e} = \frac{\gamma_e}{2\pi} = \gamma$. Plugging γ_{0_e} into Eqn. 45 yields $\gamma_0 = \mu_0\gamma_{0_e} = \mu_0\frac{\gamma_e}{2\pi}$. It is important to bring up that $\frac{\gamma_e}{2\pi}$ is not equivalent to γ due to the 2π conversion factor in $\frac{\gamma_e}{2\pi}$. By multiplying by 2π on both sides of Eqn. 45, one can get the correct values for γ_0 from γ_{0_e}. This does not mathematically change any units.

Thus, it can be claimed that the conversion from γ_{0_e} seen across numerous pieces of literature to γ_0 used in Ubermag requires the conversion as shown in Eqn. 46.

$$2\pi\gamma_0 = 2\pi\mu_0\gamma_{0_e} \tag{46}$$

Again, the 2π in front of γ_0 is a conversion factor. It is required to correct γ_{0_e} to be compatible with γ_0. While Eqn. 46 gets the correct units, it still is not quite there in order to be useful for Ubermag. There is one other definition where $\gamma_L = \frac{\gamma_0}{1+\alpha^2}$. Ubermag uses this γ_L, thus the final correction factor is given in Eqn. 47. This can take a gyromagnetic ratio value in terms of $\frac{Hz}{Oe}$ and place it in the form that will properly work within Ubermag.

$$\gamma_0 = 2\pi\mu_0\frac{\gamma_{0_e}}{1+\alpha^2} \tag{47}$$

APPENDIX F FIRST PRINCIPLES MATLAB CODE

```
%Created By: 1st Lt Michael Sherburne
%Date: 4/20/2022
%Description: User can input material parameters of magnetic nanocrystals
%in order to simulate their FMR peak.

close all
clc
clear

%User Inputs
Hint = 177; %Internal Magnetization of the Particle (Oe)
Hdc = 1000; %Applied DC Magnetic Field (Oe)
alpha = .246; %Alpha Dampening Factor
r = 7.5e-9; %Nanoparticle Radius (m)
MsUser = 102.24; %Magnetization saturation (emu/g)
p = 5.18; %Density of material (g/cm^3)
K1 = 1.36E4; %1st Order Anisotropy Constant (J/m^3)
Aex = 13.2e-12; %J/m Exchange Energy
Ge = 2.0; %G-Factor
fLow = 1e1; %Lower Frequency to Sweep To
fHigh = 10e9; %Upper Frequency to Sweep To
fStep = 10e3; %Frequency Step Size

%Constants
u0 = 1.256E-6; %Permeability of a Vacuum (H/m)

%Calculation/Preparation Steps
dia = r.*2; %Nanoparticle Diameter (m)
V = (4/3).*pi.*r.^3; %Volume of Nanoparticle (m^3)
K = K1/2; %Divide K1 by 2 to get an average aniostropy
Ms = ((MsUser)*(p)*1000); %Magnetization saturation
Hk = (2*K)/(1*Ms); %Anisotropic Magnetization (A/m)
H0 = (Hint+Hdc)*79.577471546; %Applied Magnetic Field (A/m)

%Derive Gamma from 1st Principles Using QED
echarge = 1.602e-19; %Charge of an Electron (C)
me = 9.1093837015e-31; %Electron Rest Mass (kg)
hbar = 1.054571817e-34; %Planck's Constant (Js)
beta = (echarge*hbar)/(2*me); %Bohr magnetron
gamma = ((((Ge*beta)/hbar)*(1/(2*pi)))/1E4); %Hz/Oe
gamma = gamma/79.577471546; %m/As
f =fLow:fStep:fHigh; %Frequency Sweep (Hz)
ximagFreq = f;

%Susceptibility equations are in terms of Hz instead of w to simplify math
xx = (gamma.*(H0+(1)*Hk)-i.*(alpha./1).*f);
Xxx = (((gamma.*Ms).*xx)./((gamma.*(H0+(1)*Hk)-i.*(alpha./1).*f).^2-f.^2))./(4*pi);

%Frequency FMR Plot [100]
%%%%%%%%%%%%%%%%%%%%%%%%%%%%%%%%%%%%%%%%%%%%%%%%%%%%%%%%%%%%%%%%%%%%%%%%%%%%
```

```
figure
    yyaxis('left');
    plot(f./1E9,real(Xxx),'LineWidth',3)
    ylabel('$\rm \chi \prime$ (a.u.)','Interpreter',...
            'latex','FontSize',30)
    yyaxis('right');
    plot(f./1E9,imag(Xxx),'LineWidth',3)
    ylabel('$\rm \chi \prime \prime$ (a.u.)','Interpreter',...
            'latex','FontSize',30)
    grid on
    grid minor
    xlabel('Frequency (GHz)','Interpreter',...
        'latex','FontSize',30)

%FFT Response
%%%%%%%%%%%%%%%%%%%%%%%%%%%%%%%%%%%%%%%%%%%%%%%%%%%%%%%%%%%%%%%%%%%%%%%%%%%%
  %FFT power spectrum (P = sqrt(x^2+y^2))
    figure
      plot(f./1E9,sqrt(abs(Xxx).^2)./max(sqrt(abs(Xxx).^2)),'LineWidth',3)
      ylabel('FFT Power (a.u.)','Interpreter',...
            'latex','FontSize',30)
      grid on
      grid minor
      xlabel('Frequency (GHz)','Interpreter',...
      'latex','FontSize',30)

%%%%%%%%%%%%%%%%%%%%%%%%%%%%%%%%%%%%%%%%%%%%%%%%%%%%%%%%%%%%%%%%%%%%%%%%%%%%
%Find Peak FFT Power Frequency
%%%%%%%%%%%%%%%%%%%%%%%%%%%%%%%%%%%%%%%%%%%%%%%%%%%%%%%%%%%%%%%%%%%%%%%%%%%%
ximag = max(sqrt(abs(Xxx).^2)./max(sqrt(abs(Xxx).^2)));
ximagLoc = find(sqrt(abs(Xxx).^2)./max(sqrt(abs(Xxx).^2)) == ximag);
ximagFreq = ximagFreq(ximagLoc)
```

APPENDIX G UBERMAG PYTHON CODE

```
#Import Packages
import discretisedfield as df
import micromagneticmodel as mm
import oommfc as mc

#For Post-Process Plotting
import matplotlib.pyplot as plt
import numpy as np

#Set Simulation Parameters
NumUnitCell = 4 #Number of Unit Cells Per Direction
r = 15e-9/2 #Nanoparticle Radius (m)
UnitCell = (r*2)/NumUnitCell #Unit Cell Size (m)
MsUser = 102.24 #emu/g
K1 = 1.36e4/2 #J/m^3 (Lee 2021 paper has it divided by 2 for an average)
Aex = 13.2e-12 #J/m
Hint = 0 #Internal Magnetic Field of Fe3O4 Nanoparticle (Oe) #Lee's paper used
#num modeling to get Hint, did not use it in input
Hdc = 1000 #Applied DC Field (Oe)
alphaUser = 0.246
gammaUser = ((2.8e6/(1+alphaUser**2))/(10**(-4)))*mm.consts.mu0*2*np.pi #Hz/Oe -> m/As
Hac = 5*79.5774715459 #A/m
pFe3O4 = 5.18

#Process Variables
Ms = MsUser*pFe3O4*1000 #emu/g * g/cm^3 -> 1 emu/cm^3 ->
#1000 A/m <- major effect on peak
Hk = (2*K1)/Ms
Hstatic = (Hint+Hdc+Hk)*79.5774715459 #A/m

UserCell =  (UnitCell,UnitCell,UnitCell)  # mesh discretisation (m)
def norm_fun(point):
    x, y, z = point

    if x**2 + y**2 + z**2 <= r**2:
        return Ms
    else:
        return 0

#Create Mesh
mesh = df.Mesh(p1=(-r, -r, -r), p2=(r, r, r), cell=UserCell)
m_init = df.Field(mesh=mesh, dim=3, value=(0, 0, 1), norm=norm_fun)
m_init.plane('x').mpl()
m_init.norm.k3d.nonzero()
system = mm.System(name='nanosphere',T=0) #Specify finite temperature here

#Ground State Energy Setup
system.energy = (mm.Exchange(A=Aex) +
                 mm.Demag() +
                 mm.CubicAnisotropy(K=K1, u1=(1, 0, 0), u2=(0, 1, 0)) +
```

```
                    mm.Zeeman(H=(0,0,Hstatic)))  # put DC field here
system.energy
system.m = m_init
system.dynamics = mm.Precession(gamma0=gammaUser) + mm.Damping(alpha=alphaUser)
system.dynamics
md = mc.MinDriver()
md.drive(system)
system.m.plane('z').mpl()
system.energy += mm.Zeeman(H=(Hac,0,0), func='sinc', f=10e9, t0= 30e-9, name='ac')
td = mc.TimeDriver()
td.drive(system, t=100e-9, n=2000,n_threads = 20)
system.table.data.plot('t', 'mx')
fft = system.table.rfft()
susceptibility =  (fft.data['ft_mx']*Ms)/((fft.data['ft_Bx_ac']/1e3) \
/(mm.consts.mu0))/(np.pi*4)    from scipy.signal import find_peaks
lst = -1*np.imag(susceptibility)
peaks, _ = find_peaks(lst, height=.1)
print(peaks)
freqpeak = np.array(fft.data['f'])
print(freqpeak[peaks]) #Frequency Peak of X''

#Create Susceptibility Plot

fig, ax1 = plt.subplots()

ax1.set_xlabel('Frequency (GHz)')
ax1.set_ylabel('Real (X)', color = 'red')
ax1.plot((fft.data['f']/1e9),np.real(susceptibility), color = 'red')
plt.ylim((-0.5,1))
ax1.tick_params(axis ='y', labelcolor = 'red')
ax2 = ax1.twinx()

ax2.set_ylabel('Imaginary (X)', color = 'blue')
ax2.plot((fft.data['f']/1e9),-1*np.imag(susceptibility), color = 'blue')
ax2.tick_params(axis ='y', labelcolor = 'blue')
plt.xlim((0,10))
plt.ylim((0,.9))
plt.show()

#FFT Power
plt.plot(fft.data['f']/1e9,np.sqrt(np.abs(susceptibility)**2) \
/np.max(np.sqrt(np.abs(susceptibility)**2)))
plt.title('FFT Power')
plt.xlabel('Frequency (GHz)')
plt.ylabel('FFT Power (a.u.)')
plt.xlim((0,10))
plt.show()

lst = np.sqrt(np.abs(susceptibility))**2/np.max(np.sqrt(np.abs(susceptibility)**2))
peaks, _ = find_peaks(lst, height=.4)
freqpeak = np.array((fft.data['f']))
print(freqpeak[peaks]) #Frequency Peak of X''
```